Structure of ^{120}Te from the ^{118}Sn(α,2$n\gamma$) reaction and ^{120}I decay

J. R. Vanhoy,* R. T. Coleman, and K. A. Crandell
Department of Physics, United States Naval Academy, Annapolis, Maryland 21402, USA

S. F. Hicks, B. A. Sklaney, and M. M. Walbran
Department of Physics, University of Dallas, Irving, Texas 75062, USA

N. V. Warr and J. Jolie
Institut für Kernphysik, Universität zu Köln, D-50937 Köln, Germany

F. Corminboeuf,† L. Genilloud,‡ J. Kern,§ and J.-L. Schenker
Physics Dept., University of Fribourg, CH-1700 Fribourg, Switzerland

P. E. Garrett
Lawrence Livermore National Laboratory, Livermore, California 94551, USA
(Received 16 June 2002; revised manuscript received 25 February 2003; published 18 September 2003)

The level structure of ^{120}Te has been examined utilizing gamma-ray spectroscopy following the (α,2$n\gamma$) reaction and ^{120}I decay. Excitation functions, γ-γ coincidences, and angular distributions were measured. Spectroscopic information, e.g., spins, branching ratios, and multipole-mixing ratios, was obtained for many new levels below 4.5 MeV in excitation energy. The level scheme was examined from the viewpoint of an anharmonic vibrator model, the general collective model, the particle-core coupling model, and interacting-boson-model-based intruder models. Particular aspects of the level sequence can be reproduced by each of these models, but the agreement with transition rate data is modest. The $B(E2)$ transition rate ratios are most consistent with the simple U(5) pattern. The higher-spin intruder states are identified in ^{120}Te by comparison to the known band structures and decay patterns of the $N=66$ and $N=68$ tin and cadmium nuclei. The intruder signature vanishes below spin-8, where there is strong mixing between states.

DOI: 10.1103/PhysRevC.68.034315 PACS number(s): 25.40.Fq, 27.60.+j, 23.20.−g, 21.60.Ev

I. INTRODUCTION

At first glance, tellurium-120 appears to be a good candidate for a quadrupole vibrational nucleus (Fig. 1). The two-phonon triplet and three-phonon quintet of states seem readily apparent. The splittings between members of these multiplets are reasonably small, suggesting that a spherical vibrational model would provide a good description of the nuclear properties. As such, the tellurium isotopic chain should be a good testing ground for vibrational models and their perturbations.

As erroneous conclusions can be drawn from studies of an isolated nucleus, we consider the isotopic chain (Fig. 1) to uncover the active structures in this region. Away from the midshell ^{118}Te, anharmonicities increase. Toward the heavier Te nuclei, the energies of the 2_1^+, 4_1^+, and 2_2^+ states increase as expected and the 0_2^+ state rapidly rises to join the 3_1^+ state. Other trends are not expected for a sequence of vibrational nuclei. The 6_1^+ state drops to nearly constant energy above $A=122$ instead of maintaining its position near the 3_1^+ and 4_2^+ states. This behavior suggests particlelike components in the 6_1^+ state wave function [1–3].

Rotational bands are observed in the neighboring Sn and Sb nuclei, where configurations based on $g_{9/2}$ holes are associated with nuclear deformation and produce rotational band structures. These intruder configurations [4] are thought to be observed in all the neighboring nuclei Cd [5], Sn [6,7], Sb [6], and I [8]; however, the situation for the tellurium nuclei is not as clear.

Previous experimental information on ^{120}Te mainly concerns intermediate spin states from a ^{110}Pd(^{13}C,3$n\gamma$) measurement [9], ^{118}Sn(α,2n) [10,11], and several ^{120}Iβ^+/electron capture (EC) decay measurements [11,12]. A full evaluation of the National Nuclear Data Center (NNDC) data sets was recently completed by Kitao *et al.* [13]. The present study was undertaken to add additional low-spin spectroscopic information (spins, branching ratios, and multipole-mixing ratios) in the region above the two-phonon multiplet, thereby providing a basis for evaluating anharmonic vibrator model, particle-core coupling model, and interacting-boson-model (IBM)-based intruder model descriptions.

In Sec. II we briefly describe the experimental procedures used to extract level and transition information, and in Sec. III we discuss those states for which there is special concern about the interpretation of the data. Section IV contains detailed comparisons of the experimental information to various model predictions. Our results are summarized in Sec. V.

*Email address: vanhoy@usna.edu
†Present address: Hospital Sion, Sion, Switzerland.
‡Present address: Asulab, Marin, Switzerland.
§Deceased.

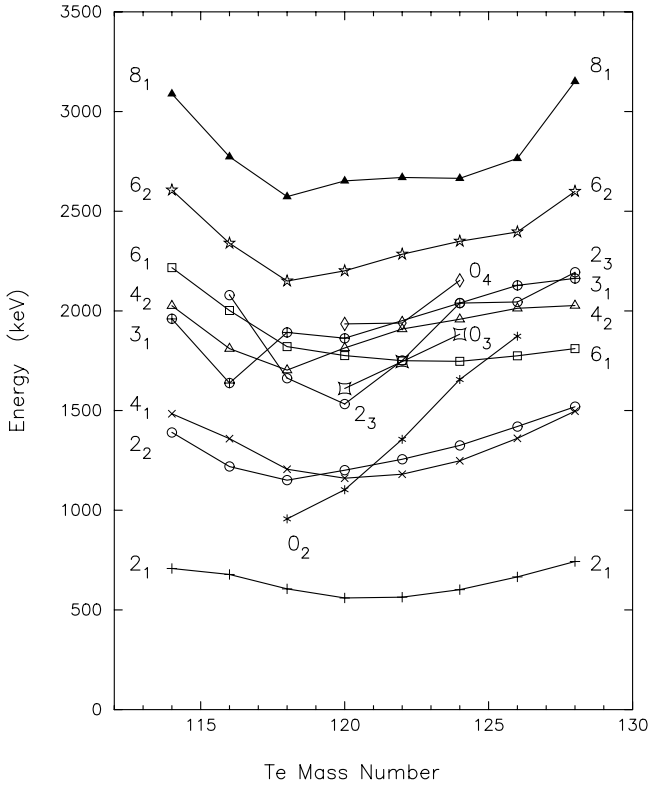

FIG. 1. The mass dependence of selected energy levels in the tellurium nuclei. The 2_1^+, 4_1^+, and 2_2^+ states show the expected spacing and parabolic increase expected for vibrational states as the neutron number varies from midshell. For neutron numbers above midshell, the 6_1^+ state remains at nearly constant excitation energy, suggestive of an underlying particle structure.

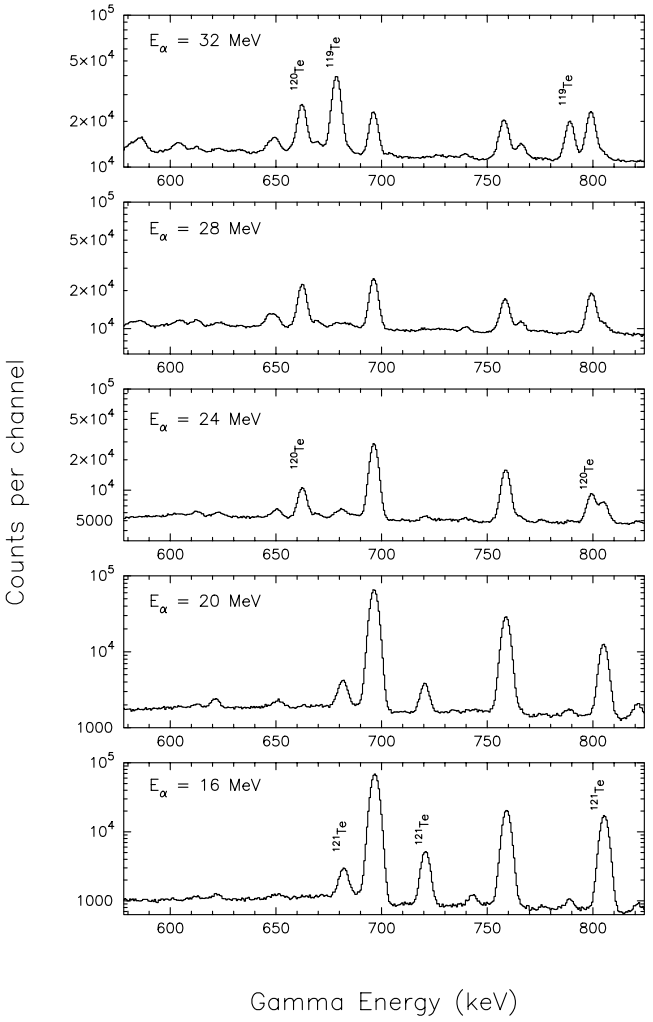

FIG. 2. Samples of singles γ-ray spectra from the ^{118}Sn$(\alpha,xn\gamma)$ reaction at different alpha-particle energies, E_α. Several lines have been labeled with their residual nucleus assignment.

II. EXPERIMENTAL METHODS

Measurements were performed at the Paul Scherrer Institute, Villigen, Switzerland using α and ^{14}N beams from the Philips variable-energy cyclotron. γ-ray excitation functions and angular distributions were measured in-beam following the (α,xn) reaction on ^{118}Sn foil targets of 95.75% isotopic enrichment and 7 mg/cm^2 thickness. A Compton-suppressed intrinsic Ge detector of 130 cm^3, as described in Ref. [14], was utilized to obtain singles spectra (Fig. 2).

Two types of coincidence measurements were performed using a system comprising five Compton-suppressed intrinsic Ge detectors [15]. In-beam γ-γ coincidence measurements were made following the ^{118}Sn(α,xn) reaction. γ-ray coincidences were also recorded from an activated ^{120}I sample which was prepared with the ^{110}Pd(^{14}N,4n) reaction on 99% isotopically enriched targets of 5 mg/cm^2 thickness.

The level scheme of ^{120}Te was constructed from the coincidence measurements. The ^{120}I decay measurements provide access to the lower-spin states, $J=0-4$, of the nucleus, and most of the level scheme was constructed by analysis of this cleaner β-decay data. Coincidences from the $(\alpha,2n)$ reaction tend to populate states with spins 6–12 directly. For that reaction, lower-spin states are observed as a result of the deexciting cascades.

Spin assignments for ^{120}Te were obtained from $(\alpha,2n\gamma)$ ten-point angular distribution measurements performed at $E_\alpha=24$ and 28 MeV. In order to extract the magnetic substate alignments (σ), level spin, and $E2/M1$ mixing ratio δ, we followed the procedures described by both Der Mateosian and Sunyar [16] and Cejnar and co-workers [17,18]. The σ's were found to have a slight excitation energy dependence, as expected [18]. (A sample of the der Mateosian procedure for extracting σ from a mixed $E2/M1$ transition from a spin-4 state is illustrated in Fig. 3.) The mixing ratios provided in Table I are from the latter Cejnar-Kern method, which takes perturbations on the angular correlations from γ-ray feeding into account.

Excitation functions were measured at five incident α-particle energies and serve several purposes. First, the shape of the γ-ray excitation function reflects the energy dependence of the $1n$, $2n$, or $3n$ exit channel and can be used to assign transitions to the proper final nucleus (Fig. 4). Second, the slope of an individual excitation function is somewhat sensitive to the spin of the parent state [19] and serves as a consistency check on the spin assignment. Because the angular distributions were measured at two ener-

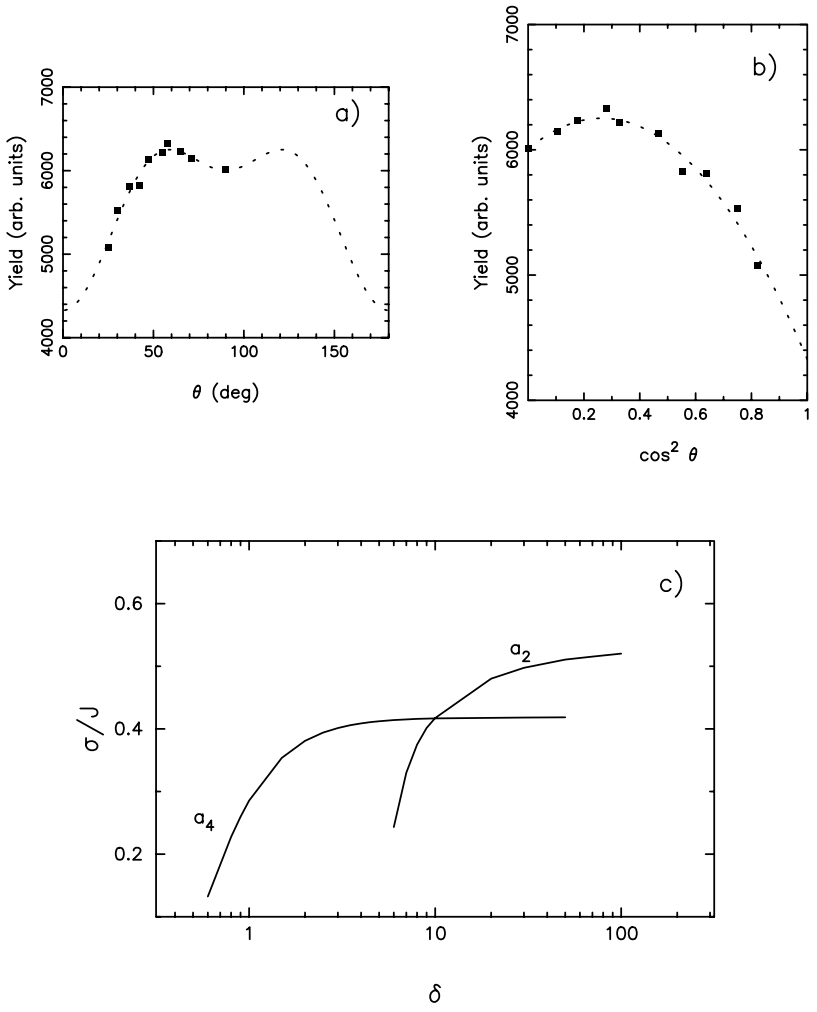

FIG. 3. Angular distribution data and analysis of the previously known $4_2 \rightarrow 4_1$ transition. Spins and mixing ratios are extracted following the procedures described in Refs. [12,17,18]. For mixed-multipolarity transitions, both alignment parameter σ and mixing ratio must be extracted from the data simultaneously. Analysis of each Legendre coefficient provides a series of (δ,σ) values. The common solution occurs where the a_2 and a_4 curves intersect.

gies, the efficiency-corrected A_0 values from the Legendre polynomial fits can be used for refined values of the excitation function slope, defined as

$$SL = \frac{200}{E_2 - E_1} \frac{A_{0_2} - A_{0_1}}{A_{0_2} + A_{0_1}}. \quad (1)$$

γ rays emitted from the same level should have consistent values of SL, provided there are no complicating effects from doublet lines in the spectrum.

The activated ^{120}I sample also provided an opportunity to estimate log *ft* values. Singles spectra were recorded in 10-min intervals during the ^{120}I decay measurements. Sample γ-ray decay curves (yield versus time) extracted from these data are shown in Fig. 5. In ^{120}I, the 2^- ground state is accompanied by an unresolved isomer of unknown spin (4–8) [20]. The two states have very similar half-lives of 81 and 53 min, respectively. Decays from the 2^- state populate primarily states of spins 0–4 in ^{120}Te, while decays from the higher-spin isomer tend to populate spins 4–8. The measured decay curve can be expressed as a superposition of the decay curves from the ground and isomeric ^{120}I states. The effective decay time T_{decay} for each γ-ray decay curve is then related to the relative contribution of the two components and thus allows one to produce log *ft* estimates. In cases where there is an unambiguous interpretation, the log *ft* values can be used to confirm spin or parity assignments.

III. LEVEL SCHEME DISCUSSION

Approximately 73% of the observed transitions were readily placed into a scheme of ~100 levels using the techniques outlined above. The resulting level scheme is given in Table I along with γ-ray transition information. Branching ratios were cross checked by comparing A_0's in both the 24- and 28-MeV angular distributions with gated spectra in the coincidence measurements. Legendre coefficients and multipole-mixing ratios are provided from the 24-MeV data measurement, although both angular distributions were used in the analysis. Efficiency-corrected γ-ray intensities are presented from both the $(\alpha,2n)$ and β-decay singles data sets. The effective mean decay time T_{decay} is obtained from time analysis of the gamma-ray intensity following the ^{120}I decay and serves as another consistency check on γ-ray placements and spin assignments. Log *ft* values from the ground and isomeric ^{120}I states are given in Table II. The systematics of decays from this nucleus seem to indicate that log *ft* values in the range 7.0–8.5 have an ambiguous interpretation, while

TABLE I. Level scheme and transition information for ^{120}Te. The $E2/M1$ multipole mixing ratio δ is provided instead of multipolarity (XL) where possible. Alternate solutions for δ are listed when appropriate. The Legendre coefficients and mixing ratios provided are those extracted from the 24-MeV angular distribution. Relative γ-ray intensities, I_β and $I_{\alpha,2n}$, are taken from the ^{120}I decay yields and the $(\alpha,2n\gamma)$ reaction, respectively. T_{decay} is the decay half-life. Uncertainties are those in the last digits. In situations where the spectrum peak was obscured or too weak to extract values, the entry is left blank.

						Legendre coeff.			Rel. Intens.		
J^π	Level (keV)	E_γ (keV)	E_f (keV)	BR %	XL/δ	a_2 ($\times 10^3$)	a_4 ($\times 10^3$)	SL	I_β	$I_{\alpha,2n}$	T_{decay} (min)
2^+	560.44(3)	560.44(3)	0	100	$E2$	272(6)	−156(6)		1000	1000	62(2)
0^+	1103.03(4)	542.59(1)	560	100	$E2$	−16(11)	−83(16)	−6.0(5)	17	7.5	80(2)
4^+	1161.54(3)	601.10(1)	560	100	$E2$	847(19)	−633(18)	3.1(3)	650	750	50(1)
2^+	1201.47(6)	640.83(1)	560	69.0(16)	0.27(15)	51(33)	−374(60)		110	46	79(1)
					1.19(19)						
		1201.88(3)	0	31.0(16)	$E2$	115(12)	−86(19)	−0.3(10)	13	22	86(8)
2^+	1535.45(6)	333.90(18)	1201	9.9(10)	−1.4(13)	−532(22)	21(34)	a	<0.05	1.5	
		432.21(6)	1103	7.2(10)	$E2$				6.5		
		974.61(3)	560	39.4(5)	0.18(20)	−263(15)	−66(22)	−0.4(6)	18	8.8	77(2)
		1535.88(4)	0	43.5(5)	$E2$	99(19)	−81(27)	−1.5(11)	7.3	12	77(4)
6^+	1776.13(9)	614.59(7) [b]	1162	100	$E2$	241(2)	−241(4)	9.8(7)	480	580	47(1)
4^+	1815.75(15)	280.17(20)	1535	10(1)	$E2$						
		614.59(16) [b]	1201	57(2)	$E2$						
		653.52(4)	1162	26(2)	10.(5)	−133(6)	−138(10)	1.4(4)	12	16	54(2)
					−0.84(5)						
		1254.69(7)	560	6.8(10)	$E2$						
3^+	1863.27(13) [c]	661.85(3) [b]	1201	36.8(44)	−2.7(4)	−183(9)	23(13)	−1.2(4)	25	13	66(1)
		701.60(7) [b]	1162	23.8(51)	−3.7(10)	19(14)	−128(22)	a	5.9	7.5	78(4)
		1302.86(6)	560	39.4(64)	0.17(2)	1(11)	−43(16)	−2.3(8)	9.3	22	74(3)
4^+	1924.31(6) [c]	762.73(4)	1162	28.0(20)	8.9(10)	−84(7)	−49(11)	−0.3(4)	15	18	53(2)
		1363.88(6)	560	72.0(20)	$E2$	144(9)	−116(13)	3.0(9)	14	43	56(2)
0^+	1936.91(90) [c]	402.21(22)	1535	13.6(40)	$E2$				<1.1		
		735.28(6)	1201	81.3(100)	$E2$				4.5		87(8)
		1375.00(50)	560	5.1(30)	$E2$				<1.3		
1^+	1983.76(12) [c]	449.89(50)	1535	4.1(1)	−0.35(10)	125(21)	−142(31)		4.9		
		782.53(50)	1201	22.0(40)					<1.0		
		881.08(3) [b]	1103	3.9(11)	$M1$				3.4		
		1423.19(6) [b]	560	68.4(10)	0.27(10)	−186(15)	−39(25)	−3.3(11)	9.5	9.1	82(3)
(4−8)	2029.16(11)	253.03(7) [b]	1776						16		
4^+	2083.60(10) [c]	881.08(3) [b]	1201	3.9(11)	$E2$				3.4		
		1523.16(5)	560	96.1(68)	$E2$	451(33)	−754(56)	−2.3(6)	4.0	13	82(3)
3^+	2104.70(10)	1544.26(7)	560	100	−0.21(9)	−178(37)	79(54)	−2.0(15)	12	5.7	71(3)
6^+	2201.39(7)	384.92(20)	1816	3.1(1)	$E2$						
		425.32(3)	1776	35.6(2)	0.07(2)	276(2)	−83(3)	11.0(2)	10	43	66(1)
					0.58(3)						
		1039.83(3)	1162	61.2(3)	$E2$	239(3)	−147(4)	11.2(6)	51	158	46(1)
(1−3)	2234.68(18)	1673.24(18)	560	100		−299(95)	47(155)	-2.0(26)	1.9	1.8	87(8)
(4−6)	2357.98(18)	1196.44(18)	1162	100		248(22)	9(35)	0.8(11)	13	15	49(3)
5	2422.25(22)	498.99(75)	1924	5.8(20)	−0.96(40)	−749(31)	133(45)	6.3(6)	<1.6	1.9	
		1260.71(22)	1162	94.2(12)	−1.86(10)	−456(8)	198(12)	1.3(7)	6.6	32	49(4)
(5)	2445.02(18)	1283.48(18)	1162	100	−8.6(28)	−116(18)	106(26)	−3.6(12)	6.7	12	56(3)
(3)	2457.16(9) [c]	1255.65(9)	1201						14		69(4)
		1895.77(13)	560			−89(83)	100(127)		3.3	2.7	
5^-	2461.08(17)	1299.54(16)	1162	100	$E1$	−359(5)	16(8)	4.2(6)	9.3	59	55(3)
3^-	2463.00(9)	1876.00(13)	560	100	$E1$	−152(54)	−29(86)	−3.2(20)	3.3	4.1	87(11)
3^+	2494.84(19)	1934.40(19)	560	100	−0.78(60)	−471(74)	421(113)	−5.8(25)	3.5	3.1	64(6)
6^+	2520.05(15)	704.60(13)	1816	37.0(10)	$E2$	241(9)	−172(14)	7.2(4)	9.3	13	47(2)

TABLE I. (*Continued*).

						Legendre coeff.			Rel. Intens.		
J^π	Level	E_γ	E_f	BR	XL/δ	a_2	a_4	SL	I_β	$I_{\alpha,2n}$	T_{decay}
		743.74(6)	1776	63.0(5)	−0.47(1)	83(8)	−83(12)	6.6(5)	16	22	51(2)
					1.4(2)						
3^+	2612.93(10) [c]	529.04(18)	2084	3.7(20)					2.2		87(12)
		750.71(7)	1863	11.0(11)	-0.47(10)	−5(63)	−21(94)	6.8(15)	3.0	3.0	
		1411.13(6)	1201	16.5(30)		−16(20)	−25(26)		17	12	80(7)
		1450.97(57)	1162	68.8(5)	−2.15(20)	93(10)	−39(16)	1.8(8)	5.2	17	80(7)
8^+	2652.97(24)	452.20(20)	2201	1.8(1)	*E*2						
		876.84(22)	1776	98.2(1)	*E*2	74(4)	−228(5)	15.2(4)	6.3	220	44(3)
(0–3)	2689.69(11)	2129.25(11)	560						6.0		
3^+	2723.80(15)	860.53(6)	1863	100	−0.09(9)	97(31)	−131(48)	2.2(12)	0.9	4.2	
(2–4)	2749.12(10)	1548.41(30)	1201	19(3)					1.5	1.0	78(9)
		2188.24(7)	560	81(4)				−2.9(77)	11	0.3	83(4)
(2–5)	2749.30(8) [c]	886.00(50)	1863	100					1.5	0.10	
5^+	2778.00(24)	852.94(86)	1924	28.7(30)	5.6(15)	−87(34)	−111(54)	7.5(10)	2.3	3.2	69(7)
		1616.46(24)	1162	71.3(30)	−0.84(30)	−1032(23)	121(36)	0.4(12)	4.0	9.0	53(4)
5^-	2792.00(18) [c]	1631.00(18)	1162	100	*E*1	−418(15)	21(24)	1.0(10)	2.0	15	53(8)
6^+	2807.11(15)	1030.98(13)	1776	100	−0.58(2)	27(15)	30(22)	5.3(7)	11	12	51(3)
8^+	2835.13(12) [c]	633.80(13) [b]	2201	9(1)	*E*2				7.5	24	53(3)
		1058.99(3)	1776	91(4)	*E*2	329(5)	−72(7)	7.6(4)	52	51	47(1)
	2835.63(24) [c]	477.65(15)	2358	100		330(26)	129(35)	10.1(5)	4.9	2.3	49(4)
5(3,4)	2842.25(16)	1680.71(13)	1162	100	−14(5)	−68(29)	84(44)	2.7(13)	1.4	6.8	63(4)
3^+	2869.85(21) [c]	1668.38(19)	1201	100	*M*1	−762(163)	261(280)	a	2.9	1.0	67(6)
(6^-)	2878.14(18) [c]	417.06(6) [c]	2461	100		a			<0.3	1.1	
7^-	2899.11(37)	1122.98(37)	1776	100	*E*1	−332(3)	−26(5)	11.0(4)	4.0	72	59(4)
3^+	2937.19(6) [c]	854.0(14) [b]	2084								
		1074.54(50)	1863						1.3	<0.1	
		1402.27(22) [b]	1535						10.0		
		1775.81(9)	1162						8.2	3.9	
		2376.43(10)	560			−582(96)	−100(149)		7.5	2.7	
7^+	2940.18(15)	739.32(13)	2201	23.8(3)	−0.22(10)	−396(9)	−53(14)	11.6(1)	3.0	17	
					−0.57(20)						
		1163.88(13)	1776	76.2(5)	−1.04(30)	−977(34)	567(51)	9.4(5)	12	78	46(2)
(0–4)	2962.95(8)	2402.51(7)	560								
(4^+)	2963.66(15)	1101.36(12)	1863	90.9(10)	1.0(4)	258(10)	−76(15)	7.1(6)	6.1	20	71(5)
		1762.42(15)	1201	9.1(10)		−444(100)	−243(159)	3.2(24)	5.9	2.2	66(3)
6^+	2972.12(24)	452.07(19)	2520	100	1.37(20)	125(21)	−142(31)	23.1(5)	3.8	2.5	46(4)
(4–8)	2975.5(20)	1199.4(20) [b]	1776	100		−217(43)	43(26)		1.3	3.4	
(7^-)	3030.39(11)	828.52(4)	2201	12.5(6)	*E*1	−477(12)	−103(20)	11.74(61)	1.1	8.3	
		1254.33(4)	1776	87.5(5)	*E*1	−335(5)	−17(8)	10.6(5)	12	59	69(4)
8^+	3039.08(10)	837.69(3)	2201	100	*E*2	251(2)	−195(4)	16.7(4)	1.7	91	
	3043.37(15)	841.98(14)	2201	100					8.2	10	46(2)
(3)	3052.52(50)	1517.07(50)	1535	100	1.3(7)	175(101)	175(137)	16.7(1)	1.0	2.1	
(6–8)	3070.03(24) [c]	417.06(6) [b]	2653	100					<0.3	1.2	
7^+	3110.48(12)	909.03(9)	2201	35(1)	0.09(1)	−134(19)	−86(30)	a	12	7.0	47(2)
		1334.38(6)	1776	65(1)	0.75(25)	409(40)	−79(58)	2.7(22)	24	8.9	47(1)
6^+	3122.12(9) [c]	1345.99(3)	1776	100	2.1(3)	6(36)	−88(53)	2.7(13)	150	5.4	46(3)
$(6–8)^+$	3122.21(9) [c]	287.00(10)	2835.1	28(4)		−401(21)	34(26)		5.0	1.1	53(3)
		920.85(4)	2201	72(7)					26	12	50(1)
(0–4)	3124.74(19)	1923.27(18)	1201	100					5.1		67(5)
8^+	3130.83(13)	295.70(6)	2835.1	100	−0.58(4)	74(5)	−55(5)	8.5(1)	13	23	48(1)
$5^{(-)}$	3141.61(9)	940.22(7)	2201	100	(*E*1)	−362(13)	−26(20)	6.4(7)	1.8	13	55(6)
(8^-)	3142.24(16)	111.65(6)	3030	18.1(1)	−0.73(3)	−5(4)	−62(7)	15.1(1)	<0.05	1.3	

TABLE I. (*Continued*).

						Legendre coeff.			Rel. Intens.		
J^π	Level	E_γ	E_f	BR	XL/δ	a_2	a_4	SL	I_β	$I_{\alpha,2n}$	T_{decay}
		202.12(6)	2940	30.3(1)	$E1$	−374(7)	−59(10)	15.5(1)	<0.05	2.2	
		243.16(6)	2899	52.0(1)	0.47(1)	386(6)	7(9)	14.3(1)	<0.05	3.8	
$(6-8)^+$	3159.08(30)	322.18(27)	2835.1	100					1.2		76(14)
5^+	3163.66(43)	2002.12(43)	1162	100	−1.2(9)	−489(74)	−166(143)	−4.1(28)	2.0	2.4	75(9)
(8)	3179.39(21)	344.23(16)	2835.1	100		−195(80)	−335(123)	11.2(7)	2.4	0.45	58(7)
(4−8)	3181.47(8) [b]	661.85(3) [b]	2520	6.3(40)							
		979.85(19)	2201	3.2(10)	6.3(31)				3.6		58(4)
		1405.20(4)	1776	90.5(5)	0.29(8)	129(30)	11(46)	1.1(13)	77	4.7	46(1)
7(5)	3215.53(16)	1439.40(13)	1776	100	−4.6(12)	−257(26)	84(46)	−1.9(14)	7.8	4.6	53(2)
					−0.18(10)						
5^+	3217.60(24)	1401.85(18)	1816	100	−8(4)	−1276(64)	−59(181)	10.8(23)	9.1	1.1	62(3)
6^+	3226.15(18)	1024.76(16)	2201	100	1.31(20)	132(12)	−165(18)	8.6(7)	0.45	13	
(2−6)	3257.02(16)	2095.48(16)	1162	100					1.5	0.41	
(2−6)	3263.15(75)	1061.76(75)	2201	100					1.1	0.8	
(1−5)	3286.47(13)	537.82(75)	2749.1			140(22)	−131(33)	−18.7(7)	0.4	3.2	
		1423.19(4) [b]	1863								
6^+	3320.15(37)	209.67(36)	3110	6.6(1)	−1.3(3)	−124(22)	−59(31)	−7.2(2)	1.3	0.6	62(6)
		1119.1(16)	2201	93.4(6)	0.8(2)	264(18)	−143(27)	−2.2(1)	5.9	7.7	44(3)
(4)	3341.97(9)	729.18(9) [b]	2613						6.5	18	71(4)
		1566.08(43)	1776			−434(16)	33(23)	5.2(10)	0.4	15	
		2140.44(30)	1201						2.9		
		2180.19(16) [b]	1162			164(161)	31(248)	0.1(35)	5.3	1.5	97(7)
10^+	3364.37(27)	325.15(1)	3039	72.6(8)	$E2$	272(3)	−180(4)	20.1(1)		20	
		711.77(12) [b]	2653	27.4(6)	$E2$	219(13)	−184(19)	25.3(1)		14	
1(3)	3371.47(22)	2170.00(22)	1201	100	−0.8(5)	−547(179)	−18(302)	4.4(36)	4.4	1.3	80(6)
9^-	3374.08(24)	721.11(3)	2653	100	$E1$	−391(4)	−23(7)	18.3(3)	1.6	31	
$(5,7)^{(+)}$	3396.54(37)	1620.41(37)	1776	100	$(M1)$	−364(29)	−163(45)	5.3(12)	2.0	7.4	
9^-	3399.67(27)	360.67(4)	3039	15(5)	$E1$	−480(11)	−25(16)	13.7(4)	<0.05	4.5	
		746.69(6)	2653	85(2)	$E1$	−335(6)	−30(10)	16.6(4)	14	23.5	
(5−7)	3450.82(19)	572.68(7)	2878	100		−44(02)	−391(12)	11.7(3)	0.4	13	89(33)
$6(7)^+$	3484.87(19)	1283.48(18)	2201	100	1.4(4)	125(34)	−239(51)		6.9	8.2	56(4)
(5−9)	3486.09(75)	545.91(75)	2940	100							
(8)	3487.53(15)	356.70(4)	3130	100	1.4(2)	78(6)	−61(9)	12.8(2)	<0.05	6.4	
					−0.60(4)						
(3,4)	3493.00(28)	743.74(4) [b]	2749.1	91.7(9)					14.9		51(2)
		2291.66(19)	1201	8.3(3)	$E1$	−859(132)	338(191)	−3(13)	2.5	2.0	
(1−4)	3541.37(28)	2339.90(28)	1201	100					1.3		
10^+	3543.67(24)	890.70(4)	2653	100	$E2$	199(5)	−178(8)	21.1(4)		34	
	3564.31(26) [c]	729.18(9) [b]	2835.1	100		212(4)	−180(5)	12.0(16)		50	
9	3566.65(25)	913.68(10)	2653	100	$E1$	−294(11)	−34(17)	16.4(5)	<1.2	13	
	3605.09(19)	482.88(17)	3122.2	100							
	3633.98(41)	313.83(14)	3320	100		−332(50)	159(73)	25.9(4)	2.5	0.6	55(4)
	3653.66(45)	614.58(45)	3039	100							
	3665.03(45)	1801.76(45)	1863	100							
	3701.85(45)	671.46(6)	3030	100							
	3813.07(15)	671.46(6)	3141	100							
	3833.35(11)	909.03(9) [b]	1924								
	3990.45(38)	2214.32(38)	1776	100				−1.9(45)		2.9	71(7)
11^-	4086.49(27)	686.82(13)	3400		$E2$	401(36)	−292(53)	33.8(5)		2.9	
		711.77(12) [b]	3374		$E2$						
(12^+)	4092.60(28)	728.23(7) [b]	3364	100	$E2$	212(4)	−180(5)	12.0(16)	a	70	

TABLE I. (*Continued*).

						Legendre coeff.			Rel Intens.		
J^π	Level	E_γ	E_f	BR	XL/δ	a_2	a_4	SL	I_β	$I_{\alpha,2n}$	T_{decay}
	4099.78(33)	2323.65(32)	1776								
	4267.36(93)	723.69(93)	3544								
	4458.89(41)	1623.26(33)	2835.1								
12^+	4459.76(29)	916.09(17)	3544	100	$E2$	262(29)	−133(42)	28.8(7)		5.4	
8(7,9)	4552.39(43)	1716.76(36)	2835.1								
	4693.7(14)	1150.0(14)	3544								
	4817.87(32)	725.27(9)	4093								
	5344.47(35)	526.60(12)	4818								

[a]Value not provided because of a difficulty in either the 24- or 28-MeV spectrum peak.
[b]The transition is a doublet or greater.
[c]See text for discussion.

values lower and higher are representative of transitions with no parity change.

Approximately 40 new low-spin levels were identified below 4.0 MeV excitation (compared to the previous count of 60). No evidence was found for 1613, 2423, 2428, 2567, 3036, 3136 keV levels listed in the NNDC compilation [13] as a result of revised placement of γ rays. Three previously reported levels at 2749, 2937, 2963, and 3112 keV are observed to be doublets.

For a few states, the analysis is of special concern. Those cases are discussed below.

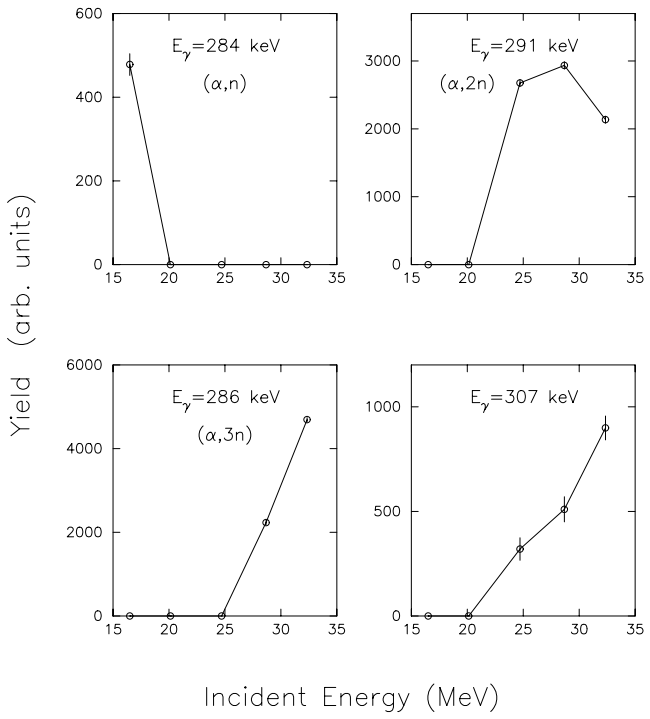

FIG. 4. A selection of excitation functions. Reaction kinematics and penetrabilities give each (α,xn) channel a different energy dependence. The transitions of 284, 291, 286 keV are placed in the nuclei ^{121}Te, ^{120}Te, ^{119}Te, respectively. The 307-keV transition is a doublet with components belonging to both the ^{119}Te and ^{120}Te nuclei.

The former 1613-keV state. The existence of this 0^+ state would have profound consequences for the nuclear structure interpretation. The 1053(1)-keV transition reported in the NNDC compilation is observed in the activated-sample datasets, but it is in coincidence with other lines that can be attributed to the decay of an ^{118}Sb contaminant. No ^{120}Te transitions feeding this level are found.

The 1924-keV 4^+ *state*. The 1364-keV line may have a small contribution from another γ ray. The angular distributions of both γ rays deexciting this level indicate a spin of either 3 or 4; however, decay patterns from the higher lying 2422-keV level strongly suggest the 1924-keV state should be spin-4. The higher-spin preference is also supported by the excitation function slope SL. The effective decay times T_{decay} of both γ's are also very similar to the other 4^+ states in this system. Our $a_2 = -0.087(7)$ for the 763-keV transition rules out the spin-2 assignment given in the compilation [13].

The 1937-keV 0^+ *state*. Transitions belonging to the 1937-keV state are only observed in the β-decay data and as such indicate a low spin. The level is not strongly fed from high-spin decay cascades or it would be more apparent in the (α,2n) data. The T_{decay} of the 735-keV transition indicates that this state is only fed from the 81-min 2^- ground state, which also indicates low spin.

The 1984-keV 1^+ *state*. Coincidence data indicate that there are four transitions originating from this level. The angular distributions of the 450-keV and 783-keV transitions do not provide definitive spin information. The 881-keV and 1423-keV lines are doublets. The major portion of the 1423-keV peak belongs to this level, and its angular distribution indicates a preferred spin-1 or -3 solution. Considering all transitions and SL, the best spin assignment is 1. The nonzero δ of the 1423-keV transition indicates positive parity.

The 2084-keV 4^+ *state*. The strong positive $a_2 = 0.451(33)$ and negative a_4 for the 1523-keV transition rules out the negative parity assignment given in the compilation [13].

The 2457-keV (3) state. Reliable information is obtained only from the β-decay data. The 1256-keV transition is present in the (α,2n) reaction data, but the peak is domi-

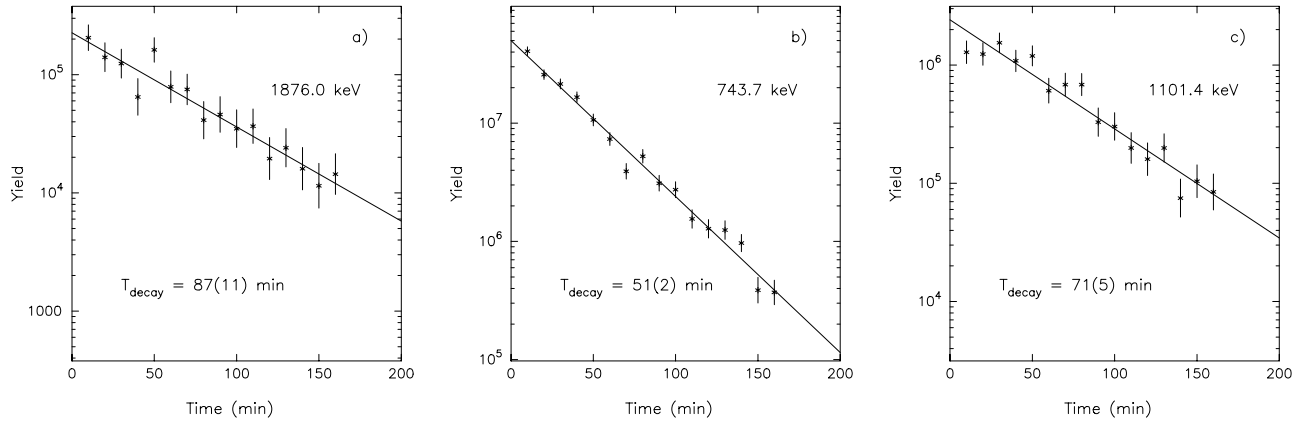

FIG. 5. A selection of ^{120}I γ-ray decay curves. (a) The 1876.0-keV γ-ray transition from the 2463-keV level has a characteristic decay time T_{decay} indicating it is populated by β decay primarily from the 2^- ^{120}I ground state and therefore has spin 0–4. (b) The T_{decay} of the 743.7-keV γ-ray transition indicates the 2520-keV level is populated primarily by decay from the ^{120}I isomer and therefore has spin 4–8. (c) The T_{decay} of the 1101.4-keV γ-ray transition indicates the 2964-keV level is populated from both ^{120}I states and therefore has an intermediate spin.

nated by a close line from the 3030-keV level. As a result there is no useful information from the angular distribution measurement. T_{decay} indicates the state is populated from both 53- and 81-min ^{120}I states, and therefore has a probable spin of 3 or 4. The weak a_2 of the 1896-keV transition suggests the best choice is spin-3.

The 2613-keV 3^+ *state*. Four transitions originate from a level at this excitation energy; 529, 751, 1411, and 1451 keV as identified by gating on the 729-keV feeder transition. Both 529-keV and 1451-keV lines have T_{decay} consistent with decay from the ^{120}I 2^- ground state. The 1411-keV peak may be a doublet in the $(\alpha,2n)$ excitation function and angular

TABLE II. Log *ft* values extracted from the ^{120}I decay experiment. Hyphens indicate that the decay branch is clearly absent.

	Log *ft*			Log *ft*	
State	Gnd st	Isomer	State	Gnd st	Isomer
1936.91	8.2(1)	-	2899.11	-	7.8(1)
1983.76	7.7(1)	-	2937.19	7.2(1)	
2083.60	8.1(1)	9.3(1)	2940.18	-	7.3(1)
2104.70	7.9(1)	8.5(1)	2963.66	7.4(1)	7.8(1)
2201.39	-	7.3(1)	2972.12	-	7.9(1)
2234.68	8.5(1)	-	3030.39	-	6.7(1)
2357.98	-	7.8(1)	3043.37	-	7.5(2)
2422.25	-	8.2(1)	3110.48	-	6.7(1)
2445.02	8.6(1)	8.1(1)	3122.12	-	6.2(1)
2457.16	7.7(1)	8.2(1)	3122.21	-	6.9(1)
2461.08	8.7(1)	7.9(1)	3124.74	7.7(2)	8.1(2)
2463.00	9.8(1)	-	3141.61	8.9(1)	8.2(1)
2520.05	-	7.3(1)	3142.24	-	7.6(1)
2612.93	7.2(1)	-	3159.08	8.2(1)	9.2(1)
2652.97	-	7.9(1)	3163.66	8.0(2)	8.8(2)
2689.69	7.7(1)	-	3179.39	-	8.1(1)
2749.12	7.4(1)		3215.53	-	7.5(1)
2778.00	8.3(1)	7.9(1)	3217.60	9.2(1)	7.4(1)
2792.00	9.9(4)	8.3(1)	3371.47	7.5(1)	-
2807.11	-	7.5(1)	3396.54	-	9.2(2)
2835.13	-	7.8(1)	3450.82	8.3(2)	-
2835.63	-	6.8(1)	3484.87	-	7.4(3)
2842.25	8.2(2)	8.2(2)	3633.98	-	7.7(1)
2869.85	8.2(1)	-	3990.45	7.5(2)	8.0(2)

distribution data. The 529-keV line was weak in the (α,2n) singles measurements. Fits to the 751-keV and 1451-keV angular distributions require spin-3.

The 2749.3-keV state. The 886-keV transition is cleanly observable only in coincidence data. This transition could belong to the known level at 2749.1 keV, but it was not obviously present in gated spectra feeding that level.

The 2792.00-keV 5^- *state*. The angular distribution indicates a spin of 5. The log *ft* from the ^{120}I ground state is large, 9.9(1), and similar in size to the analogous transition for the 3_1^- state. Negative parity has been assigned to this 2792-keV state.

The 2835.1-keV 8^+ *and 2835.6-keV states*. A close pair of levels lies at an excitation energy of 2835 keV, and γ rays of 478, 634, and 1058 keV are involved in the decays. The combination of singles and coincidence measurements indicates that the 634-keV peak is a doublet. Placements are made by examining coincidences on the deexciting and feeding transitions into the pair of levels. Branching ratios are derived from the gates on the feeding transitions. Singles data indicate that practically all of the 633.8-keV γ-ray yield in the 24-MeV data belongs to an alternate source, and much of it in the 28-MeV dataset too. The 633.8-keV line's $SL=-23.2(3)$ indicates that this strong component belongs to the (α,n) channel (decay of the ^{121}Te $11/2^-$ isomer). The decay gate on the 633.8-keV line shows a significant 634.1-keV peak (not placed) and thus the coincidence intensities are suspect.

The 2870-keV 3^- *state*. The 1668-keV transition is obvious in the lower energy singles and decay coincidence data, but is not observed in the 28-MeV singles and (α,2n) coincidence measurements. This would suggest a low spin. The effective decay time, however, indicates that it is produced from both states in ^{120}I and thus should have an intermediate spin. The angular distribution is consistent with a dipole transition.

The 2878-keV and 3070-keV states. Each of these levels decays only by the emission of a 417-keV γ ray. The coincidence measurements suggest that both 2878- and 3070-keV levels are strongly populated by the (α,2n) reaction. The 2878-keV level also appears in previous (^{13}C,3$n\gamma$) and (α,2$n\gamma$) studies, where it was assigned spin 6^-; however, in those data the strongly populated 3070-keV level was not indicated. Hence, we are unable to confirm the previous 6^- assignment. The 417-keV transition is very weak in the decay coincidence measurement and its gated spectrum suggests a third placement independent of the first two.

The 2937-keV state. Five γ rays (854, 1075, 1402, 1776, and 2376 keV) are observed to originate from levels at 2937-keV excitation. The previously tabulated ground-state transition was not observed [20]. Our coincidence data are unable to demonstrate that all five originate from the same state. The relative yields of the 1075, 1776, and 2376-keV transitions are consistent over $E_\alpha=16$–32 MeV and thus indicate they depopulate the same level. The spectral 1402-keV peak is a doublet with most of its yield coming from the higher 3218-keV level. A spin-3 assignment is required to fit the decay pattern.

The 3122-keV states. Based on coincidence data, two states are found to occur at 3122-keV excitation. Previously in Ref. [21] only one was suggested. A very strong 1346-keV transition which feeds the 1776-keV 6^+ level is observed in the β-decay data. This transition is relatively weak in the (α,2n) measurements. Two weaker 287- and 921-keV transitions are also observed, but these belong to a separate 3122-keV level as indicated from spectra gated on the 483-keV feeding transition. The 287 and 921-keV lines are not apparent in the singles measurements. The log *ft* values from decay of the isomer for both states are <7.0 and this suggests positive parity.

The 3181.5-keV state. The 1405-keV transition had been previously placed from a 2566-keV state [20,21]. In our β-decay γ-γ coincidences for the 1405-keV gate, we observe the 560, 601, and 614-keV peaks all with similar yield. We find no evidence for the 2567-keV level in either (α,2n) or ^{120}I decay datasets. The 980-keV line has been placed with the 3181-keV state based on energy considerations.

IV. MODEL DISCUSSION

The nucleus ^{120}Te lies near the center of the $N=50$–82 shell and the level scheme is strongly suggestive of a harmonic vibrator. To uncover the actual underlying structures, we have considered a variety of models. The positive-parity levels of ^{120}Te are shown in Fig. 6.

We first examine this nucleus within the constraints of the IBM, then move to the general collective model (GCM), and finally to treatments including particlelike character of the excitations and $2p$-$2h$ excitations.

The level structures derived from the various models discussed in the following sections are displayed in Fig. 6, while transition rates are compared in Table III. Unfortunately only the level lifetime of the first excited state is known. One can still get a feeling for the preference of decays if one looks at the $B(E2)$ branching ratios from a level.

A. Anharmonic vibrator descriptions

As ^{120}Te appears to be a vibrational nucleus, we begin by considering the appropriateness of the ''anharmonic vibrator'' which was first shown to be equivalent to the U(5) limit of the IBM-1 by Aprahamian *et al.* [22].

The eigenvalues may be written [23] as

$$E=\epsilon n_d+\alpha n_d(n_d+4)+\beta\nu(\nu+3)+\gamma L(L+1), \quad (2)$$

where n_d is the number of d bosons, ν is the number of d-bosons pairs not coupled to zero angular momentum, and L is the total angular momentum of the state. The Hamiltonian parameters were extracted by fitting the nine levels of the 1-, 2-, and 3-quadrupole multiplets. Acceptable fit parameters are found to be $\epsilon=587.7\pm0.3$ keV, $\alpha=-5.84\pm0.19$ keV, $\beta=9.23\pm0.19$ keV, and $\gamma=1.85\pm0.19$ keV. The resulting level scheme is shown in Fig. 6. Transition rates were calculated with PHINT [24] and are given in Table III. It is observed that the calculated states decay in a pure multiphonon fashion (Fig. 7). The agreement is quite acceptable as all large $B(E2)$ ratios are predicted to be large and all small ratios small in a consistent fashion.

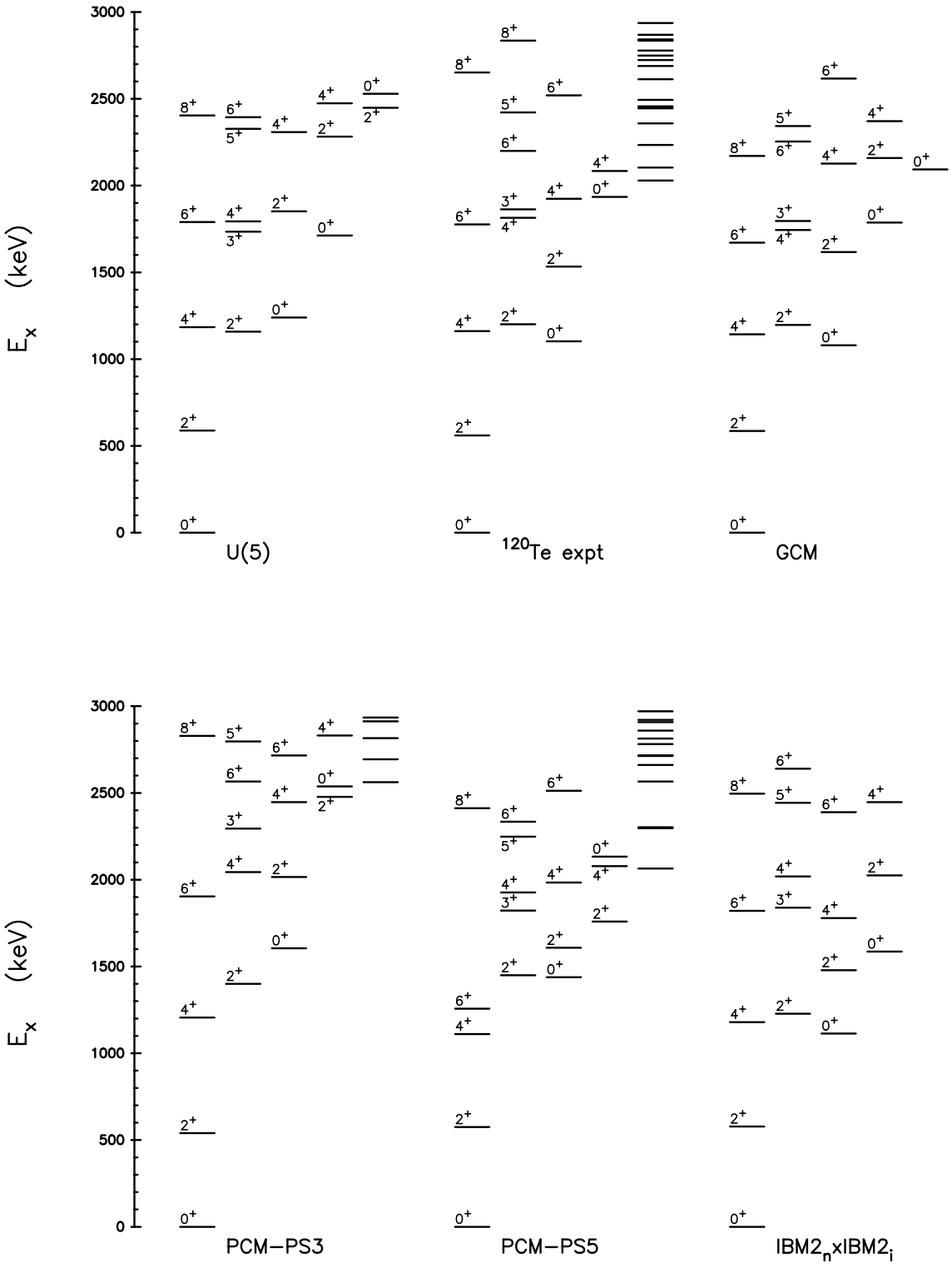

FIG. 6. Comparison of the experimental ^{120}Te level scheme with model calculations. The organization of levels into columns is purely for clarity and does not imply a particular physical interpretation. Additional low-spin levels present are indicated in the fifth columns.

The general collective model [25–28] may also be used to provide an empirical description of the quadrupole collective motion of nuclei described by the radial shape function

$$R(\theta,\phi,t)=R_0\left[1+\sum\ \alpha^*_{\lambda\mu}(t)Y_{\lambda\mu}(\theta,\phi)\right], \qquad (3)$$

with $\lambda=0,2$ and where $\alpha_{\lambda\mu}$ are the time-dependent multipole deformation parameters. The Hamiltonian is constructed in terms of the $\alpha_{\lambda\mu}$ and the corresponding canonical momenta. The Gneuss-Greiner form of potential energy may be expressed in terms of the standard polar intrinsic deformation variables β and γ,

TABLE III. $B(E2)$ transition rate ratio comparisons for ^{120}Te.

Ratio	This expt.	U(5)	GCM-GG[a]	PCM-PS3[b]	PCM-PS5[c]	Intruder[d]
$\frac{2_2-2_1}{2_2-0_1}$	3.2 or 27.6	∞	1.3	1.1	0.48	100
$\frac{2_3-2_2}{2_3-2_1}$	179	∞	175	0.68	0.0010	45
$\frac{3_1-2_2}{3_1-2_1}$	879[e]	∞	0.0072	34	95	45
$\frac{3_1-2_2}{3_1-4_1}$	1.97	2.5	0.0023	4.5	86	
$\frac{4_2-2_2}{4_2-2_1}$	12000	∞	5.2	6.0	28	5700
$\frac{4_2-2_2}{4_2-4_1}$	3.0	1.1	43	1.4	8.1	1.6
$\frac{0_2-2_2}{0_2-2_1}$		0	0.47			1.2
$\frac{0_3-2_2}{0_3-2_1}$	370	∞	6.2	310	0.12	6.4
$\frac{0_3-2_3}{0_3-2_2}$	3.48	0	0.25	0.028	1.5	

[a]Gneuss-Greiner formulation of the General Collective Model.
[b]PCM calculation of Ref. [35].
[c]PCM calculation using PS5 and transition rate parameters as discussed in text.
[d]Intruder mixing caluclation from Ref. [56].
[e]Mixing ratio value for the $3_1^+-2_2^+$ transition is suspect.

$$V(\beta,\gamma)=C_2\sqrt{\frac{1}{5}}\beta^2-C_3\sqrt{\frac{2}{35}}\beta^3\cos(3\gamma)+C_4\frac{1}{5}\beta^4 - C_5\sqrt{\frac{2}{175}}\beta^5\cos(3\gamma)+C_6\frac{2}{35}\beta^6\cos^2(3\gamma) + D_6\sqrt{\frac{1}{125}}\beta^6. \quad (4)$$

This model has the feature that all types of macroscopic collective behavior are treated as one. The first three terms are sufficient to describe most collective behavior; the last three serving as higher-order refinements in the potential. Values for the six potential parameters above were derived from fits to the nine levels of the 1-, 2-, and 3-quadrupole multiplets. To ensure that the minimization routine found the absolute minimum, searches were made starting from different potential parameters selected from the Hg and Ru region [28]. Variation of C_5, C_6, D_6 had a minor effect on the level scheme and was therefore set to zero. The final potential parameters were (in MeV) $C_2=2670\pm30$, $C_3=-18\,900\pm500$, $C_4=4780\pm10$, with kinetic energy parameters $B=2924$ and $P=-0.0124$. The observed level scheme in Fig. 6 is quite nicely reproduced. The splitting pattern of states within each multiplet is qualitatively correct.

Caprio *et al.* [29] have examined the general case of vibrational multiplet splittings within the GCM. The patterns in both the 2- and 3-phonon multiplets are as expected for a potential with a slight $\cos3\gamma$ dependence (lower-spin states tend to be pushed up). The downward shift of the experimental 0_2^+ and 2_3^+ states is also consistent with a small $\cos3\gamma$ term in the potential. (See Fig. 3, Ref. [29].) These two states

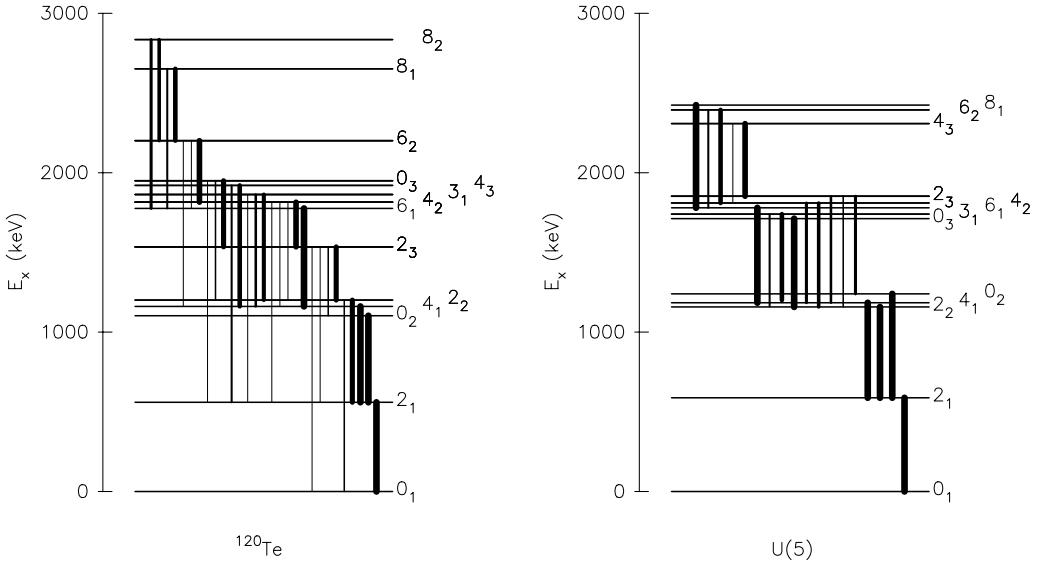

FIG. 7. Decay branchings for the low-spin levels of ^{120}Te. The $B(E2)$ for each transition is indicated by the width of the line. This width is normalized per level.

TABLE IV. PPCORE parameter sets.

Parameter set	Source/Ref.	Orbital energies (keV) $g_{7/2}$	$d_{5/2}$	$h_{11/2}$	$d_{3/2}$	$s_{1/2}$	Pairing G	Quad. Phonon $\hbar\omega_2$	Coupling ξ_2
PS1	Nilsson scheme $\epsilon=0$ [22]	0	486	1620	3070	3400			
PS2	Kisslinger [38]	0	520	2030	3190	3330			
PS3	Lopac PCM [35]	0	750	2400	1800	2000	0.25	1000	$\simeq 2.10$
PS4	Warr PCM [37]	0	1000	2030	3190	3300	0.20	1300	$\simeq 2.10$
PS5	^{119}Sb energies	270	0	1366	3130	3370	0.16	1300	$\simeq 2.25$

are ''family 2'' levels [29] and are the states that first deviate from the harmonic multiplets when the oscillator symmetry is broken in a way that maintains some γ independence [30,31].

In summary, we confirm the underlying vibrational character of ^{120}Te. Observed deviations in the 2- and 3-phonon multiplets are as expected in the GCM approach.

B. Particle structures

One can often gain deeper information on the particle versus collective structure of the excited states by use of a particle-core coupling model (PCM) [32], where, for the case of ^{120}Te, two valence protons orbit a vibrating core formed by the neutrons. We have observed (Fig. 1) that the 6_1^+ state has behavior suggestive of strong particlelike components in its wave function for the neutron-rich Te isotopes. The PCM model has been effective in understanding the two-valence $N=84$ nuclei [33,34]. Here we extend this calculation to ^{120}Te.

Several related calculations were performed some years ago on various tellurium nuclei by Lopac [35], Degriek and Van der Berghe [36], and Warr *et al.* [37]. The calculations principally differ in their choice of single-particle orbital energies (as displayed in Table IV). For the present ^{120}Te investigation, we use the code PPCORE of Copnell and Heyde, described in Refs. [32,34]. The complete PCM Hamiltonian and details required for parameter selection can be found in Refs. [34] and [37]. We present results from a corrected version of PPCORE [39,40]. (A problem was found in the code which caused PPCORE to use a smaller model space for the calculation of transition rates compared to that for the energies.)

Previous parameter sets PS1-4 start from regionally valid potential parameters, which neglect the variation in single-particle energies across the tellurium chain. Of particular interest is the inversion of the $d_{5/2}$ and $g_{7/2}$ orbitals near mid-shell witnessed in the Sb isotopes. Spectroscopic factors from proton-transfer measurements, Sn(^{3}He,d), indicate that the $5/2_1^+$, $7/2_1^+$ states nearly exhaust the allowed strength of the $d_{5/2}$ and $g_{7/2}$ orbitals in the $A=113$–125 Sb nuclei [41,42]. The $h_{11/2}$ strength in the $11/2_1^-$ state is also moderately strong in those nuclei. On the other hand, the $3/2_1^+$ and $1/2_1^+$ Sb states have complex orbital structure as the spectroscopic factors to these states are low. To examine the effect of these variations, orbital energies in PS5 are taken directly from the ^{119}Sb states. The sets PS1–4 may be more appropriate for the heavier tellurium nuclei where the $d_{5/2}$ lies higher than the $g_{7/2}$ orbital.

All parameter sets have the feature that the energies of the $g_{7/2}$ and $d_{5/2}$ orbitals are distinctly below those of the $h_{11/2}$, $d_{3/2}$, and $s_{1/2}$ orbitals. This has the effect that the low-lying states are predominately composed of $g_{7/2}$ and $d_{5/2}$ protons coupled to the core vibrations. There are two approaches for selecting the proton-proton pairing strength G. One can employ a global prescription, such as $G=17.05/A\rightarrow 0.14$ [43] or $G=19.2/A-7.4\ (N\text{-}Z)/A^2\rightarrow 0.15$ [44], or simply use a fixed value $G=0.20$ [37]. Because of this uncertainty, we have adopted the approach of varying G between these limits and searching for the best fit (PS5). The quadrupole phonon energy is chosen representative of the core Sn first excited state. In our case, the energy of the quadrupole phonon is taken from ^{118}Sn, $\hbar\omega_2\simeq 1.30$ MeV. The octupole phonon was not used. Reasonable values for the particle-phonon interaction strength ξ_2 lie between $\xi_2=2.0$ and 2.6 for the tellurium nuclei [32,34,37,45]. We have adopted the approach to vary ξ_2 and search for the best fit (PS5).

Fits to the 13 actual levels: 0_{1-3}^+, 2_{1-3}^+, 3_1^+, $4_{1,2}^+$, 5_1^+, $6_{1,2}^+$, and 8_1^+ with PS5 indicate average deviations of $\sim$25–50 keV can easily be obtained with $G=0.16\pm 0.01$ and $\xi_2=2.25\pm 0.25$. These fits are illustrated in Fig. 6. Parameter sets PS3 and PS4 reproduce the ground band easily, but have large level energy deviations with the remaining ten states. Parameter set PS5 provides smaller level energy deviations for all states with the exception of 6_1^+, which is severely depressed. In all cases, the 0_2^+ level is pushed up into the level scheme, contrary to what is observed.

To gain better understanding of the problematic 6_1^+, we have started from the PS3–5 parameter sets, varied specific terms, and compared the results to the 13 actual levels mentioned above.

The choice of G directly affects the energies of the unperturbed two-proton configurations. Increasing the value for ξ_2 pulls the 2_1^+ and 4_1^+ states lower while pushing all other states higher in energy. In all cases, the 0_2^+ state lies above the 2_1^+ and 4_1^+ states, contrary to what is observed in experiment.

Examination of the 6_1^+ wave function indicates that the stronger the $d_{5/2}g_{7/2}$ component, the lower the state lies in energy. More diverse configurations (and hence more collectivity) are required to place the 6_1^+ level into the proper

position. It was found that the 6_1^+ level could be properly positioned if the $g_{7/2}$ orbital energy was increased, but unfortunately the 0_2^+, 5_1^+, and 8_1^+ energies also rose out of their proper position. The remaining ten states were relatively independent of that modification.

Electric quadrupole transition rates are a more stringent test of level structure. A proton effective charge and a core surface-stiffness parameter C_2 must be selected. Conventional guidance [34,37] suggests $e_p \sim 1.0$ and $C_2 \simeq 250$ MeV. This choice reproduces the only known transition rate in ^{120}Te, the $B(E2; 2_1^+ \rightarrow 0_1^+)$ of 31(6) W.u. The resulting transition rate ratios are presented in Table III. The general agreement of these ratios is not clearly better than that obtained with the purely collective models discussed in Sec. IV A.

C. Intruder configurations

Proton-pickup measurements [46], (t,α), leading to antimony nuclei indicate that the Sb $9/2_1^+$ state has very strong $g_{9/2}^{-1}$ character. In Sn nuclei, low-lying structures related to the $g_{9/2}$ orbital are $2p$-$2h$ excitations [47,48]. The equivalent states in the Te nuclei would have a $4p$-$2h$ structure. Nilsson model calculations performed by Heyde *et al.* [49] demonstrate that the energy required to produce these p-h pairs is greatly reduced if the nucleus acquires a slight deformation ($\epsilon \sim 0.1$–0.2). Low-lying rotational bands built on these p-h structures are well known in Sn and Sb [50,51]. These ''intruder'' structures in the midshell tellurium nuclei have proven to be elusive and are often only assigned at high spin where band structures are apparent.

To identify the intruder configurations one requires that the behavior of a band in Te be the same as in Sn and Cd. A convenient method for making the comparison utilizes plotting the ''aligned angular momentum'' versus rotational frequency [52]. In this work we will define the rotational frequency for the ith state in a particular band as

$$\hbar\omega_i = \frac{E_{i+1} - E_{i-1}}{J_{i+1} - J_{i-1}}. \tag{5}$$

We have selected decay sequences (cascades, not necessarily to be interpreted as actual bands) from the $N=66$ and $N=68$ isotones and displayed their ''signature'' behavior in Figs. 8 and 9.

Consider the neighboring $N=66$ isotones first. The ^{116}Sn cascade connecting the 9322-keV 20^+ state with the 1756-keV state in Fig. 8 has been identified as the intruder structure in that nucleus [48]. In ^{114}Cd the sequence of states built upon the 1135-keV state has been identified as the intruder structure [5] up to spin 6^+. For both ^{114}Cd and ^{116}Sn, the intruder band head appears to reside in the strongly mixed 0_2^+ and 0_3^+ states. The band structure in ^{118}Te has been analyzed in detail by Juutinen *et al.* [53]. The only cascade in ^{118}Te with similar behavior proceeds through the 6103-keV 16^+ state [53]. This ^{118}Te sequence is nearly identical to the established intruder band in ^{116}Sn until the spin drops below the 6_1^+ state, where the cascade becomes vibrational-like. Note that, for the ^{116}Sn cascade displayed, there is a branch

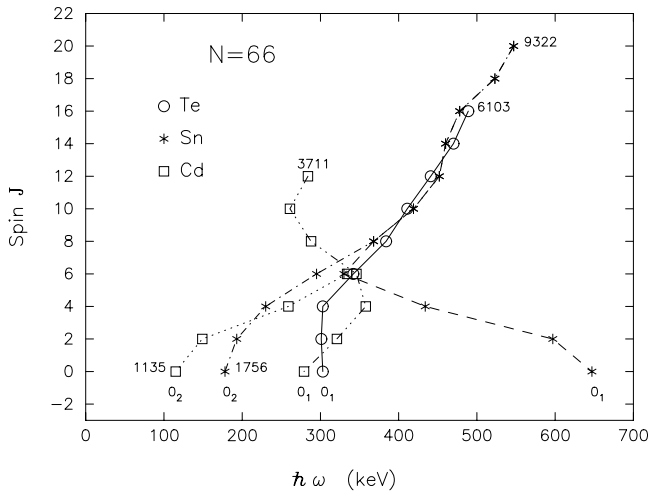

FIG. 8. Cascade signatures for $N=66$ nuclei.

point at spin 6, at which point 36% of the decay continues to the 4_2^+ state along the intruder path but 64% goes through the 4_1^+ state into the ground band.

In ^{118}Te, decay of the 1821-keV 6_1^+ state into the 1702-keV 4_2^+ state has not been observed; this would presumably complete the intruder sequence into the 0_2^+ state if the behavior of ^{118}Te is analogous to ^{116}Sn.

The $N=68$ system is examined in a similar fashion in Fig. 9. Data do not extend quite as high in spin for these nuclei. The ^{116}Cd and ^{118}Sn nuclei are very similar to $N=66$, with the intruder band head residing in the 0_2^+ state. The highest identifiable members of the intruder band are the 5379-keV state in ^{118}Sn and the 4458-keV state in ^{120}Te. ^{118}Sn again has a branch point at spin 6, at which point 63% of the decay continues to the 4_2^+ state along the intruder path and 37% goes to the ground band. In ^{120}Te, the intruder cascade disappears at spin 6. The 1776-keV 6_1^+ state drops into the 4_1^+ of the ground band, as that is the only lower-lying spin-4 state. Here an absolute lifetime measurement can distinguish between a vibrational or intruder character of this state. A careful search was made for weak transitions which could

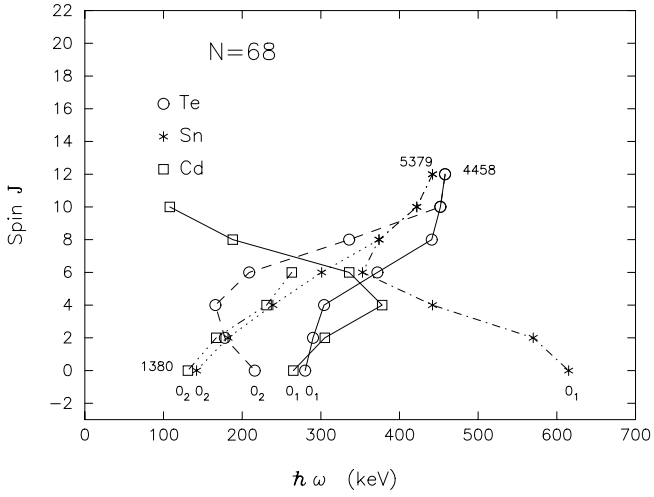

FIG. 9. Cascade signatures for $N=68$ nuclei.

lead from the 2652-keV 8^+ state into the 0_2^+ state. The two requisite transitions were located in singles data: a 452.6-keV γ-ray connecting the 8_1^+ and 6_2^+ states, and a 384.9-keV γ-ray connecting the 6_2^+ and 4_2^+ levels. Their small branching ratios, $\sim 2\%$, make confirmation difficult via coincidence measurements. This weakly connected cascade is plotted in Fig. 8, but its similarity to the intruder bands in ^{118}Sn and ^{116}Cd is not ideal. We conclude the intruder configurations are present but strongly fragmented below spin 8 in ^{120}Sn and ^{118}Te.

From Figs. 8 and 9, we notice that the ground bands begin the same for Cd and Te, but that Sn is distinctly different. Both the Cd and Te ground bands have two valence quasiparticles with respect to the $Z=50$ core ($2p$ for Te and $2h$ for Cd) and thus are fundamentally different from Sn. All these excitation sequences become similar at spin-6.

We now refer to an existing calculation, based upon the IBM formalism, for low-spin intruder states The level system is modeled by mixing a ''normal'' IBM model space with a second ''intruder'' IBM calculation [54].

A popular method for selecting the Hamiltonian parameters was followed by Rikovska *et al.* [55,56]. A ''normal'' IBM2$_n$ calculation is first performed with a standard IBM2 Hamiltonian [55]

$$H=\epsilon(n_{d\nu}+n_{d\pi})+V_{\nu\nu}+V_{\pi\pi}+\kappa Q_\pi\cdot Q_\nu+M_{\pi\nu}. \quad (6)$$

The IBM2$_i$ intruder calculation is performed with two additional proton bosons ($N_\pi+2$) representing $2p$-$2h$ excitations. The Ru and Ba nuclei were used to obtain the Hamiltonian parameters for the pure intruder configurations of IBM2$_i$. After adding an energy shift to the IBM2$_i$ states both configurations are mixed. The reader is referred to their original paper [56] for details of parameter selection and model calculations. The resulting level scheme is shown in Fig. 6, separated into anticipated band structures. The level placement is slightly improved with an average deviation of 33 keV for our 13 states. The 0_2^+ state is correctly placed below the 4_1^+ and 2_2^+ levels. From details of these IBM2$_n$ $\times$IBM2$_i$ wave functions, intruder configurations are expected to have the most impact in the states that we indicated as the ''third band'' in the experimental data: the 0_2, 2_3, 4_3, 6_3, and the 0_3 and 2_4 states. The Rikovska calculation also provides transition rates, mixing ratios, and branching ratios (see her Table II). There does not appear to be any global advantage to the introduction of the intruder configurations over the calculation with only the ''normal'' states except in the reproduction of excitation energies.

Nevertheless, these are promising developments in the understanding of intruder configurations in the midshell tellurium nuclei, and the next step would be to obtain experimental absolute transition rates for direct comparison to the model calculations.

V. SUMMARY

The level scheme of ^{120}Te has been developed utilizing γ spectroscopy following the $(\alpha,2n)$ reaction and ^{120}I decay measurements. Excitation functions, γ-γ coincidences, and angular distributions were measured. Spectroscopic information, including spins, branching ratios, and mixing ratios, was obtained for many new levels below 4.5 MeV in excitation.

The level scheme was examined from the viewpoints of the interacting boson model, the general collective model, and the particle-core coupling model. Anharmonic vibrator descriptions appear to be the most fruitful in reproducing the observed energy staggering in the phonon multiplets. The PCM model was applied with several Hamiltonian parameter sets, each with advantages and disadvantages. An attempt to connect the level directly to the spectroscopic factor information in Sb (PS5) resulted in level schemes where the 6_1^+ level was forced far below its experimental energy. Considering available transition rate data, the $B(E2)$ transition rate ratios are most consistent with the simple U(5) pattern. The intermediate-spin portion of an intruder band is identified in ^{120}Te by comparison to the known band structures of the $N=66$ and $N=68$ tin and cadmium nuclei. Because the basic nuclear structures active at ^{120}Te have similar energies, the low-spin states appear to be thorough admixtures of spherical-vibrational, two-particle, and intruder configurations. It would be of great interest to determine more lifetimes in this nucleus.

ACKNOWLEDGMENTS

This work was supported by National Science Foundation Grants Nos. PHY-0139504 and PHY-9901508 and the Swiss National Fund for Science. We also acknowledge discussions with M.T. McEllistrem and S.W. Yates of the University of Kentucky. The assistance of the Philips Cyclotron accelerator staff is sincerely appreciated.

[1] J.A. Cizewski, Phys. Lett. B **219**, 189 (1989).
[2] C.S. Lee, J.A. Cizewski, D. Barker, G. Kumbartzki, R. Tanczyn, R.G. Henry, and L.P. Farris, Nucl. Phys. **A530**, 58 (1991).
[3] I. Talmi, *Contemporary Concepts in Physics: Simple Models of Complex Nuclei* (Harwood, Chur, 1993).
[4] J.L. Wood, K. Heyde, W. Nazarewicz, M. Huyes, and P. van Duppen, Phys. Rep. **215**, 101 (1992).
[5] J. Kumpulainen, R. Julin, J. Kantele, A. Passoja, W.H. Trzaska, E. Verho, J. Vaaramaki, D. Cutoiu, and M. Ivascu, Phys. Rev. C **45**, 640 (1992).
[6] D.C. Radford, A. Galindo-Uribarri, G. Hackman, and V.P. Janzen, Nucl. Phys. **A557**, 311 (1993).
[7] M. Schimmer, R. Wirowski, S. Albers, G. Bohm, A. Dewald, A. Gelberg, and P. von Brentano, Z. Phys. A **338**, 117 (1991).
[8] E.S. Paul, C.W. Beausang, S.A. Forbes, S.J. Gale, A.N. James, P.M. Jones, M.J. Joyce, R.M. Clark, K. Hauschild, I.M. Hibbert, R. Wadsworth, R.A. Cunningham, J. Simpson, T. Davinson, R.D. Page, P.J. Sellin, P.J. Woods, D.B. Fossan, D.R. LaFosse, H. Schnare, M.P. Waring, A. Gizon, and J. Gizon, Phys. Rev. C **48**, R490 (1993).

[9] P. Chowdhury, W.F. Piel, Jr., and D.B. Fossan, Phys. Rev. C **25**, 813 (1982).
[10] J.J. Van Ruyven, W.H.A. Hesselink, J.A. Ajjermans, P. Van Nes, and H. Verheul, Nucl. Phys. **A380**, 125 (1982).
[11] W.G. Wycoff and J.E. Draper, Phys. Rev. C **8**, 796 (1973).
[12] R.A. Warner and J.E. Draper, Phys. Rev. C **1**, 1069 (1970).
[13] K. Kitao, Y. Tendow, and A. Hashizume, Nucl. Data Sheets **96**, 241 (2002).
[14] V.A. Ionescu, J. Kern, C. Nordmann, S. Olbrich, and Ch. Rhême, Nucl. Instrum. Methods **163**, 395 (1979).
[15] N. Warr, S. Drissi, J. Jolie, J. Kern, H. Lehmann, S.J. Mannanal, J.-L. Schenker, J.-P. Vorlet, and P.E. Garrett, Nucl. Phys. **A620**, 127 (1997).
[16] E. Der Mateosian and A.W. Sunyar, At. Data Nucl. Data Tables **13**, 391 (1974).
[17] P. Cejnar and J. Kern, Nucl. Phys. **A561**, 317 (1993).
[18] J. Kern, P. Cejnar, and W. Zipper, Nucl. Phys. **A554**, 246 (1993).
[19] J. Kern, A. Bruder, S. Drissi, V.A. Ionescu, and D. Kusnezov, Nucl. Phys. **A512**, 1 (1990).
[20] R. B. Firestone, V. S. Shirley, C. M. Baglin, S. Y. F. Chu, and J. Zipkin, *Table of Isotopes*, 8th ed. (Wiley-Interscience, New York, 1998).
[21] A. Hashizume, Y. Tendow, and M. Ohsima, Nucl. Data Sheets **52**, 641 (1987).
[22] A. Aprahamian, D.S. Brenner, R.F. Casten, R.L. Gill, and A. Piotrowski, Phys. Rev. Lett. **59**, 535 (1987).
[23] A. Arima and F. Iachello, Ann. Phys. (N.Y.) **99**, 253 (1976).
[24] O. Scholten, in *Computational Nuclear Physics 1: Nuclear Structure*, edited by K. Langanke, J. A. Maruhn, and S. E. Koonin (Springer-Verlag, New York, 1991), p. 88.
[25] J. M. Eisenberg and W. Greiner, *Nuclear Theory*, 3rd ed. (North-Holland, Amsterdam, 1987), Vol. 1.
[26] P.O. Hess, M. Seiwert, J.A. Maruhn, and W. Greiner, Z. Phys. A **296**, 147 (1980).
[27] D. Troltenier, J. A. Maruhn, and P. O. Hess, in *Computational Nuclear Physics 1: Nuclear Structure*, (Ref. [24]).
[28] D. Troltenier, J.A. Maruhn, W. Greiner, V. Velazquez-Aguliar, P.O. Hess, and J.H. Hamilton, Z. Phys. A **338**, 261 (1991).
[29] M.A. Caprio, R.F. Casten, and J. Jolie, Phys. Rev. C **65**, 034304 (2002).
[30] L. Wilets and M. Jean, Phys. Rev. **102**, 788 (1956).
[31] G. Rakavy, Nucl. Phys. **4**, 289 (1957).
[32] K. Heyde and P.J. Brussaard, Nucl. Phys. **A104**, 81 (1967).
[33] J. Copnell, S. Robinson, J. Jolie, and K. Heyde, Phys. Lett. B **222**, 1 (1989).
[34] J. Copnell, S.J. Robinson, J. Jolie, and K. Heyde, Phys. Rev. C **46**, 1301 (1992).
[35] V. Lopac, Nucl. Phys. **A155**, 513 (1970).
[36] E. Degrieck and G. Van den Berghe, Nucl. Phys. **A231**, 141 (1974).
[37] N. Warr, S. Drissi, P.E. Garrett, J. Jolie, J. Kern, H. Lehmann, S.J. Mannanal, and J.-P. Vorlet, Nucl. Phys. **A636**, 379 (1998).
[38] L.S. Kisslinger and R.A. Sorenson, Rev. Mod. Phys. **35**, 835 (1963).
[39] N. Warr (private communication).
[40] K. Heyde (private communication).
[41] M. Conjeaud, S. Harar, and Y. Cassagnou, Nucl. Phys. **A117**, 449 (1968).
[42] T. Ishimatsu, K. Yagi, H. Ohmura, T. Nakajima, and H. Orihara, Nucl. Phys. **A104**, 481 (1967).
[43] R.R. Chasman, Phys. Rev. C **28**, 1374 (1983).
[44] J.G. Nilsson, C.F. Tsang, A. Sobiczewski, Z. Szymański, S. Wycech, C. Gustafson, I.L. Lamm, P. Möller, and B. Nilsson, Nucl. Phys. **A131**, 1 (1969).
[45] K. Heyde, M. Waroquier, and H. Vincx, Phys. Lett. **57B**, 429 (1975).
[46] M. Conjeaud, S. Harar, M. Caballero, and N. Cindro, Nucl. Phys. **A215**, 383 (1973).
[47] J. Bron, W.H.A. Hesselink, A. van Poelgeest, J.J.A. Zalmstra, M.J. Uitzinger, H. Verheul, K. Heyde, M. Waroquier, H. Vincx, and P. van Isacker, Nucl. Phys. **A318**, 335 (1979).
[48] A. Savelius, S. Juutinen, K. Helariutta, P. Jones, R. Julin, P. Jämsen, M. Muikku, M. Piiparinen, J. Suhonen, S. Törmänen, R. Wyss, P.T. Greenlees, P. Simecek, and D. Cutoiu, Nucl. Phys. **A637**, 491 (1998).
[49] K. Heyde, M. Waroquier, H. Vincx, and P. van Isacker, Phys. Lett. **64B**, 135 (1976).
[50] A. Gaigalas, R.E. Shroy, G. Schatz, and D.B. Fossan, Phys. Rev. Lett. **35**, 555 (1975).
[51] R.E. Shroy, A.K. Gaigalas, G. Schatz, and D.B. Fossan, Phys. Rev. C **19**, 1324 (1979).
[52] R. Bengtsson and R. Frauendorf, Nucl. Phys. **A327**, 139 (1979).
[53] S. Juutinen, A. Savelius, P.T. Greenlees, K. Helariutta, P. Jones, R. Julin, P. Jämsen, H. Kankaanpää, M. Muikku, M. Piiparinen, S. Törmänen, and M. Matsuzaki, Phys. Rev. C **61**, 014312 (2000).
[54] P.D. Duval and B.R. Barrett, Nucl. Phys. **A376**, 213 (1982).
[55] J. Rikovska, N.J. Stone, and W.B. Walters, Phys. Rev. C **36**, 2162 (1987).
[56] J. Rikovska, N.J. Stone, P.M. Walker, and W.B. Walters, Nucl. Phys. **A505**, 145 (1989).